Earth and Planetary Science Letters 490 (2018) 193–205

Contents lists available at ScienceDirect

Earth and Planetary Science Letters

www.elsevier.com/locate/epsl

Using tetraether lipids archived in North Sea Basin sediments to extract North Western European Pliocene continental air temperatures

Emily Dearing Crampton-Flood [a,*], Francien Peterse [a], Dirk Munsterman [b], Jaap S. Sinninghe Damsté [a,c]

[a] Utrecht University, Faculty of Geosciences, Department of Earth Sciences, P.O. Box 80.012, 3508 TA Utrecht, The Netherlands
[b] Toegepast Natuurwetenschappelijk Onderzoek (Netherlands Organization for Applied Scientific Research), Geological Survey of The Netherlands, P.O. Box 80015, 3508 TA, Utrecht, The Netherlands
[c] NIOZ Royal Netherlands Institute for Sea Research, Department of Marine Microbiology and Biogeochemistry, and Utrecht University, P.O. Box 59, 1790 AB Den Burg, Texel, The Netherlands

ARTICLE INFO

Article history:
Received 19 June 2017
Received in revised form 12 March 2018
Accepted 14 March 2018
Available online xxxx
Editor: M. Frank

Keywords:
paleoclimate
brGDGTs
coastal sediments
air temperature
Pliocene

ABSTRACT

The Pliocene is often regarded as a suitable analogue for future climate, due to an overall warmer climate (2–3 °C) coupled with atmospheric CO_2 concentrations largely similar to present values (~400 ppmv). Numerous Pliocene sea surface temperature (SST) records are available, however, little is known about climate in the terrestrial realm. Here we generated a Pliocene continental temperature record for Northwestern Europe based on branched glycerol dialkyl glycerol tetraether (brGDGT) membrane lipids stored in a marine sedimentary record from the western Netherlands. The total organic carbon (TOC) content of the sediments and its stable carbon isotopic composition ($\delta^{13}C_{org}$) indicate a strong transition from primarily marine derived organic matter (OM) during the Pliocene, to predominantly terrestrially derived OM after the transition into the Pleistocene. This trend is supported by the ratio of branched and isoprenoid tetraethers (BIT index). The marine–terrestrial transition indicates a likely change in brGDGT sources in the core, which may complicate the applicability of the brGDGT paleotemperature proxy in this setting. Currently, the application of the brGDGT-based paleothermometer on coastal marine sediments has been hampered by a marine overprint. Here, we propose a method to disentangle terrestrial and marine sources based on the degree of cyclization of tetramethylated brGDGTs (#rings) using a linear mixing model based on the global soil calibration set and a newly developed coastal marine temperature transfer function. Application of this method on our brGDGT record resulted in a 'corrected' terrestrial temperature record (MAT_{terr}). This latter record indicates that continental temperatures were ~12–14 °C during the Early Pliocene, and 10.5–12 °C during the Mid Pliocene, confirming other Pliocene pollen based terrestrial temperature estimates from Northern and Central Europe. Furthermore, two colder (Δ 5–7 °C) periods in the Pliocene MAT_{terr} record show that the influence of Pliocene glacials reached well into NW Europe.

1. Introduction

Over the past decade, branched glycerol dialkyl glycerol tetraethers (brGDGTs) have emerged as a promising class of biomarker lipids used in paleoenvironmental reconstructions (Weijers et al., 2007a). BrGDGTs are bacterial membrane lipids present in soils and peats worldwide, and their structure consists of two alkyl chains (C_{30-32}) bound by ether bonds to two glycerol moieties (Fig. 1). Individual brGDGTs are distinguished by the number and position of methyl groups (4–6) and cyclopentane rings (0–2) on the alkyl chains (Fig. 1). Weijers et al. (2007a) analyzed brGDGTs in a global set of soils, and identified significant correlations between the degrees of cyclization and methylation of brGDGTs with soil pH and mean air temperature (MAT). This observation formed the original basis for the brGDGT-based continental paleothermometer (Weijers et al., 2007a). A second brGDGT proxy builds upon the predominantly soil origin of brGDGTs; the Branched and Isoprenoid Tetraether (BIT) index measures the relative input of soil organic matter (OM) delivered to the marine environment by runoff processes (Hopmans et al., 2004). In short, the BIT index is a ratio of the most abundant brGDGTs to Crenarchaeol, an isoprenoid GDGT

* Corresponding author.
E-mail address: e.dearingcramptonflood@uu.nl (E. Dearing Crampton-Flood).

https://doi.org/10.1016/j.epsl.2018.03.030

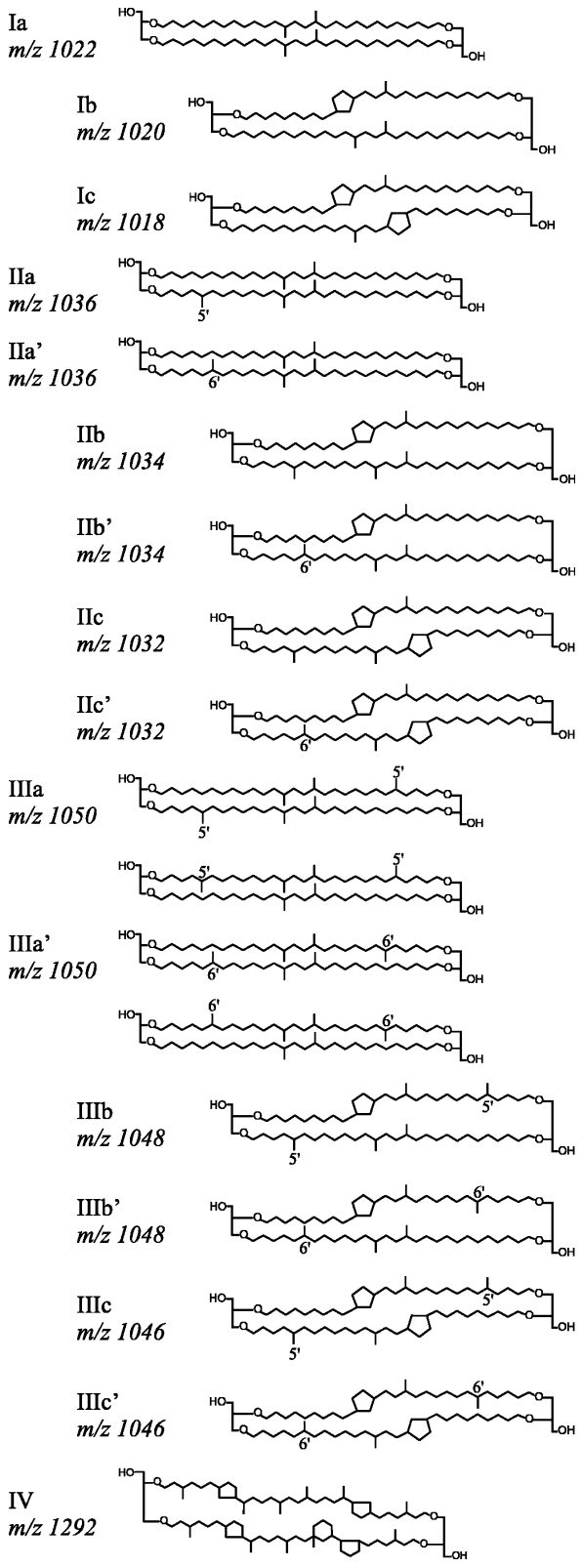

Fig. 1. Molecular structures of the brGDGTs analyzed in this study (I–III), and Crenarchaeol (IV). The tetramethylated brGDGTs are represented by structures Ia–Ic, the pentamethylated by structures IIa–IIc, and the hexamethylated by structures IIIa–IIIc. From De Jonge et al. (2014a).

produced by marine Thaumarchaeota (Sinninghe Damsté et al., 2002; Hopmans et al., 2004).

Both the brGDGT paleotemperature proxy and the BIT index have been applied in various systems throughout geological time. For example, the first MAT record based upon brGDGT-paleothemometry was carried out on a marine sediment core from the Congo River outflow, and resulted in a continuous record of tropical African continental air temperatures during the last deglaciation (Weijers et al., 2007b). Similarly, terrestrial temperature records were reconstructed for the Miocene of North Europe (Donders et al., 2009) and the mid-Pleistocene of the Arctic (de Wet et al., 2016). Application of the BIT index has also indicated the early activation of European rivers during the last deglaciation in the Bay of Biscay (Ménot et al., 2006), and served as an indirect method reflecting the amount of monsoon precipitation in Holocene sediments from Lake Challa (Verschuren et al., 2009). The BIT index is also employed in modern settings to trace OM transport from land to sea through rivers (Herfort et al., 2006).

The foundation of these brGDGT proxies is grounded in the assumption that brGDGTs are transported from the continent to coastal marine sediments by rivers and runoff. In other words, the proxies can only be suitably applied if brGDGTs in marine sediments are allochthonous components. This assumption has been challenged recently with the discovery of aquatic brGDGT production in rivers (Zell et al., 2013a, 2013b; De Jonge et al., 2014b), and coastal marine settings (Peterse et al., 2009; Sinninghe Damsté, 2016). The influence of aquatically produced brGDGTs on the paleorecord can result in a slight underestimation (up to 3 °C recorded in the Amazon river; Zell et al., 2013b), or large overestimation (up to 11–19 °C recorded in marine sediments from Svalbard; Peterse et al., 2009) of calculated MATs. Thus, a mixed source of brGDGTs in coastal marine sediments has strong implications for MAT reconstruction, as the current calibration (MAT_{mr}) is based solely upon brGDGTs in surface soils (De Jonge et al., 2014a). The wide applicability of the proxy, and thus the generation of terrestrial MAT records, is hampered by the lack of a method to disentangle these disparate sources and to correct for a possible aquatic overprint of the terrestrial brGDGT signal.

Recent analytical developments in liquid chromatography methods have permitted the discovery of structural isomers of penta- and hexamethylated brGDGTs, where the peripheral methyl group(s) varies from the 5- to the 6-position of the alkyl chain (De Jonge et al., 2013, 2014a; Fig. 1). The identification and separation of the isomers led to an improved calibration of the brGDGT paleothermometer for soils (De Jonge et al., 2014a) and aided in the recognition of riverine brGDGT production (De Jonge et al., 2015), as revealed by high abundances of pH-sensitive 6-methyl brGDGTs in suspended particulate matter (SPM) from the Yenisei River. The better match of brGDGT-based pH with the higher pH of Yenisei River water rather than the pH of the Yenisei watershed soils suggested that substantial amounts of particularly 6-methyl brGDGTs in the Yenisei River are aquatically produced.

Similarly, the number of cyclopentane rings appears to indicate in situ brGDGT production in coastal marine settings (Peterse et al., 2009; Sinninghe Damsté, 2016). In a transect of marine sediments from Svalbard, Peterse et al. (2009) observed that brGDGT concentrations increased toward the ocean, particularly those containing a cyclopentane moiety. Due to the clear offset with brGDGT distributions found in Svalbard soils, the trends in the fjord sediments could only be explained by a large contribution of in-situ produced cyclopentane-containing brGDGTs to the fjord sediments (Peterse et al., 2009). Sinninghe Damsté (2016) also observed a similar trend in two coast-shelf transects from the Berau River delta, and formulated an index based upon the weighted average number of cyclopentane moieties of tetramethylated brGDGTs, $\#rings_{tetra}$. The $\#rings_{tetra}$ shows a marked increase from the river mouth (0.22) toward the shelf break (0.83), reflecting the increased contribution of in-situ produced brGDGTs towards open sea. Thus, the new analytical method and identification of brGDGT isomers provides possibilities to disentangle soil vs. marine contributions

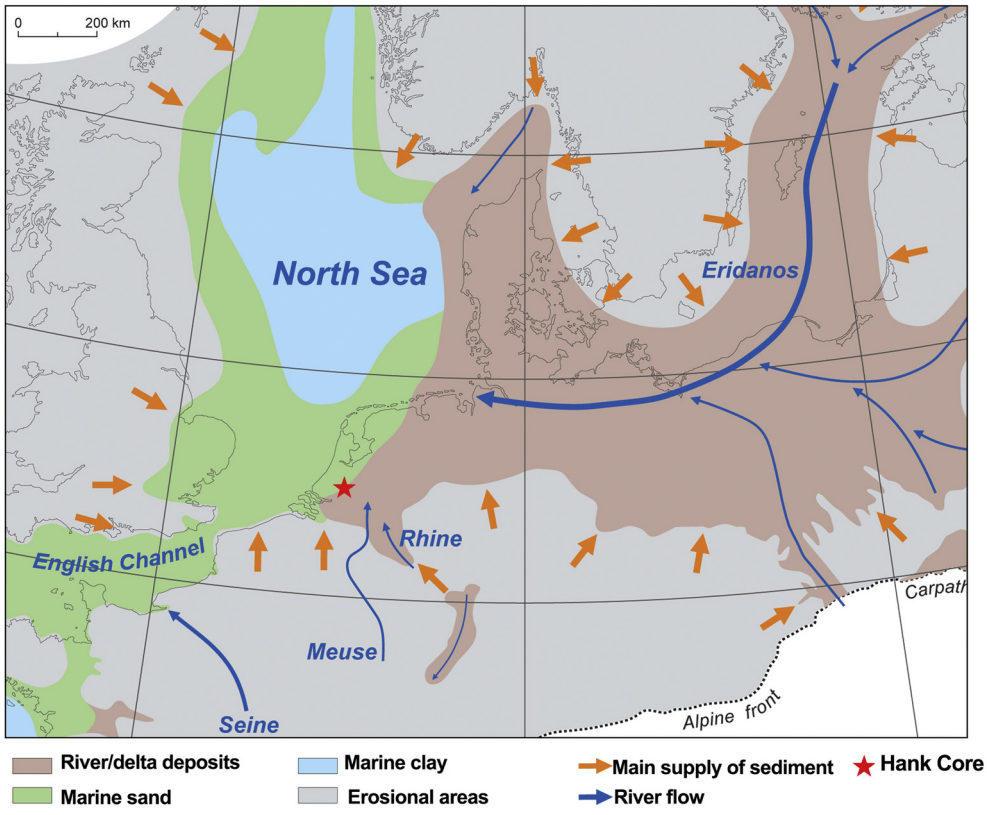

Fig. 2. Location of the Hank site in South-west Netherlands (red star). The early Pliocene paleogeography is modified after Gibbard and Lewin (2003) and Knox et al. (2010). Figure modified from Gibbard and Lewin (2016). (For interpretation of the colors in the figure(s), the reader is referred to the web version of this article.)

to the climate signal archived in coastal marine sediments, providing an opportunity to reconstruct continental MAT for areas with mixed brGDGT sources.

The North Sea basin is an ideal test case to separate marine and terrestrial sources of brGDGTs, due to its coastal location and associated sensitivity to sea level change. Here we specifically target the interval covering the Pliocene (5.33–2.58 Ma), which is the most recent geological interval possessing CO_2 atmospheric concentrations similar to both present and projected levels for the near future (400–450 ppmv, Masson-Demotte et al., 2013; Haywood et al., 2016a, 2016b). In addition, continents were in, or relatively close to, their present position (Dowsett et al., 2010; Haywood et al., 2016a, 2016b). For these reasons, the Pliocene, in particular the Mid-Piacenzian Warm Period (MPWP, 3.264–3.025 Ma; Dowsett et al., 2010) is studied to provide constraints on the magnitude and severity of future climate change.

Pliocene temperature estimates are primarily composed of sea surface temperature (SST) records generated using geochemical proxies. Comprehensive SST records of the MPWP have been compiled by the PRISM Group (Pliocene Research Interpretation and Synoptic Mapping; Dowsett et al., 1994, 2010). In contrast to the marine realm, terrestrial temperatures during the Pliocene remain poorly constrained, due to the limited number of proxies and a scarcity of continuous Pliocene terrestrial sedimentary archives. Currently, the bulk of temperature estimates are based on pollen assemblages (Head, 1998; Pross and Klotz, 2002; Meijer et al., 2006; Salzmann et al., 2008, 2013 and references therein). Although this data has been used for data-model comparison studies (e.g. Salzmann et al., 2008, 2013), there is a lack of diversity in terrestrial temperature proxies, which highlights the need for more methods to infer past terrestrial temperatures to validate the temperature estimates generated thus far.

Here we aim to extract the terrestrial temperature signal of Pliocene North-western (NW) Europe from brGDGTs and OM bulk properties archived in sediments deposited in the North Sea Basin, using the improved chromatographic method separating 5-methyl and 6-methyl brGDGT isomers (De Jonge et al., 2014a; Hopmans et al., 2016). We use the $\#rings_{tetra}$ index and end-member modeling to correct for possible changes in brGDGT sources with time. The resulting record should thus primarily represent terrestrial air temperatures, providing a semi-quantitative Pliocene air temperature record for NW Europe.

2. Methods

2.1. Study site and sampling

The study site lies within the Rhine–Meuse–Scheldt delta in North-western Europe, with a present-day climate characterized by mild, maritime conditions and an annual mean air temperature (MAT) of ~10 °C (van Engelen et al., 2001). The Hank core was drilled in 2001 in the Dutch province of Noord-Brabant (51°43′N, 4°55′E; Fig. 2) using air-lifting well technology to a base of 404 m. Samples were collected at a resolution of 1 m. The air-lifting well technology provides mixed samples for every 1 m, leading to the generation of smoothed trends in a comparatively extensive record. There was no evidence of caving observed in the core. The interval from 404 m to 136 m was selected for this study.

The lithostratigraphy of the succession spans the upper part of the Breda Formation, the Oosterhout Formation and the lower part of the Maassluis Formation (Fig. 3). The Breda Fm. consists of shallow marine glauconitic sands, silts and (sandy) clays. The Oosterhout Fm. predominantly consists of shallow to marginal marine (moderate to low glauconitic) sands and is relatively rich in shells. The Maassluis Fm. shows an alternation of shales, silts and sands

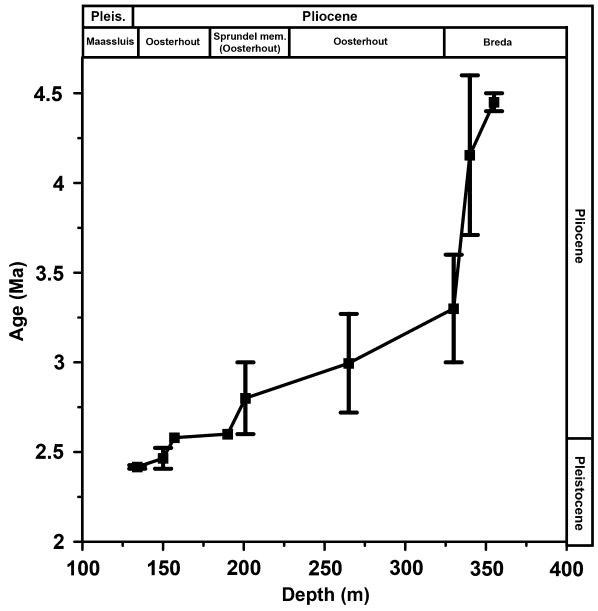

Fig. 3. Age-depth model for the Hank core, with corresponding formations. The closed squares denote Hank biostratigraphic dinocyst events summarized in Table 1. Briefly, the events are: the LOD of *Reticulatosphaera actinocoronata* (355 m), the LOD of *Operculodinium tegillatum* (340 m), the LOD of *Melitasphaeridium choanophorum* (330 m), the LOD of *Invertocysta lacrymosa* (265 m), the LOD of *Operculodinium? eirikianum* (201 m), the LOD of *Barssidinium pliocenicum* (190 m), the LOD of *Barssidinium* spp. (157 m), the acme of *Impagidinium multiplexum* (150 m), and the acme of *Operculodinium israelianum* (133–136 m).

and is developed in a near coastal shallow-marginal marine setting (Van Adrichem Boogaert and Kouwe, 1993–1997).

2.2. Palynology and age-assessment

A selection of 82 samples (~20 g) was processed for palynological analysis following the standard techniques, involving HCl and HF digestion, no oxidation, and 15 µm sieving (Janssen and Dammers, 2008). The palynomorphs were counted until 200 specimens per sample were registered. The remainder of the microscope slide was then scanned for rare species. The dinocyst taxonomy is according to that cited in Williams et al. (2017).

Ages are assigned based on last occurrence datums (LODs), first occurrence datums (FODs), and acmes of dinoflagellate cyst species in the North Sea (Table 1, Fig. 3). Key-references for the Plio–Pleistocene dinoflagellate cyst stratigraphy used for the North Sea age model are listed in Table 1. Recent stratigraphic publications on the Nordic Seas and North Atlantic are taken into account for the strong diachroneity between dinoflagellate cyst events, and applied only if discussed and correlated with their North Sea occurrences (De Schepper et al., 2015, 2017).

2.3. Bulk organic carbon analysis

Total organic carbon (TOC) content and stable carbon isotopes of the bulk OC ($\delta^{13}C_{org}$) were measured for 89 and 72 samples, respectively. Homogenized sediments were decalcified by overnight treatment with 1.0 M HCl. The samples were then rinsed 2× with demineralized water, and left to dry in an oven (60 °C). TOC content and $\delta^{13}C_{org}$ values were analyzed with a Fison NA 1500 CNS-analyzer connected to a Finnigan Mat Delta Plus isotope ratio mass spectrometer following standard procedures. TOC content values are expressed as the weight percentage of dried sediment (wt.%). $\delta^{13}C_{org}$ values are reported in the standard delta notation relative to the Vienna Pee Dee Belemnite (VPDB) standard.

2.4. GDGT extraction and analysis

In total, 155 samples were homogenized with a mortar and pestle for organic geochemical analysis. Samples (5–10 g) were extracted (3×) with dichloromethane (DCM):methanol (9:1, v/v) using an accelerated solvent extractor (ASE 350, Dionex™) at 100 °C and 7.7×10^6 Pa. Total lipid extracts (TLE) were dried under a stream of N_2. Separation into apolar, ketone and polar fractions was achieved by passing the TLE over an activated Al_2O_3 column using hexane:DCM (9:1, v/v), hexane:DCM (1:1, v/v), and DCM:methanol (1:1, v/v) as eluents, respectively. A known amount of internal standard (IS, $GDGT_{46}$) was added to the polar fraction (Huguet et al., 2006). Polar, GDGT-containing fractions were re-dissolved in hexane:isopropanol (99:1, v/v), and filtered using a 0.45 µM PTFE filter.

GDGTs were analyzed according to Hopmans et al. (2016) using an Agilent 1290 Infinity ultra high performance liquid chromatography (UHPLC) coupled to an Agilent 6130 single quadrupole mass detector. In short, separation was achieved by two silica Waters Acquity UPLC HEB Hilic (1.7 µm, 2.1 mm × 150 mm) columns at 30 °C, with a guard column of the same material preceding both. Isocratic elution was used to separate the GDGTs, starting with 82% A and 18% B for 25 min at a flow rate of 0.2 ml/min, followed by a linear gradient to 70% A and 30% B for 25 min, where A = hexane and B = hexane:isopropanol 9:1. Injection volume was 10 µL. Ionization of the GDGTs was accomplished using atmospheric pressure chemical ionization with the following source conditions: gas temperature 200 °C, vaporizer temperature 400 °C, drying gas (N_2) flow 6 L/min, capillary voltage 3500 V, nebulizer pressure 25 psi, corona current 5.0 µA.

GDGTs were identified by detecting the $[M–H]^+$ ions in selected ion monitoring (SIM) mode at m/z 1292, 1050, 1048, 1046, 1036, 1034, 1032, 1022, 1020, 1018, using m/z 744 for the internal standard. Quantitation was achieved by peak area integration of the $[M–H]^+$ ions in Chemstation software B.04.02 and comparing that with the area of the IS, assuming that the response of the mass spectrometer was similar for brGDGTs, crenarchaeol, and the IS.

Replicate measurements of a subset of samples yielded similar index values for MBT′5Me and CBT′ indices (difference <0.03 for MBT′5Me and <0.05 for CBT′), corresponding with a difference of 1.0 °C and <0.1 pH units, respectively.

2.5. GDGT proxy calculations

Roman numerals in the following equations refer to the molecular structures of GDGTs shown in Fig. 1.

The BIT index was calculated using both 5- and 6-methyl GDGTs, in an equation adapted from Hopmans et al. (2004):

$$\mathrm{BIT} = \frac{\mathrm{Ia} + \mathrm{IIa} + \mathrm{IIa'} + \mathrm{IIIa} + \mathrm{IIIa'}}{\mathrm{IV} + \mathrm{Ia} + \mathrm{IIa} + \mathrm{IIa'} + \mathrm{IIIa} + \mathrm{IIIa'}} \quad (1)$$

MBT′5Me values were calculated using fractional abundances of brGDGTs and the index defined by De Jonge et al. (2014a):

$$\mathrm{MBT'_{5Me}} = \frac{\mathrm{Ia} + \mathrm{Ib} + \mathrm{Ic}}{\mathrm{Ia} + \mathrm{Ib} + \mathrm{Ic} + \mathrm{IIa} + \mathrm{IIb} + \mathrm{IIc} + \mathrm{IIIa}} \quad (2)$$

MATs were calculated using fractional abundances of brGDGTs and the latest transfer function of De Jonge et al. (2014a):

$$\mathrm{MAT_{mr}} = 7.17 + 17.1 * [\mathrm{Ia}] + 25.9 * [\mathrm{Ib}] + 34.4 * [\mathrm{Ic}] - 28.6 * [\mathrm{IIa}] \quad (3)$$

Table 1
Biostratigraphic age model for the Hank Core. Note: ages correlating ranges for MIS 95 and 97 are based on the benthic isotope stratigraphy stack (Lisiecki and Raymo, 2005).

Dinocyst event	Depth (m)	Age (Period)	Age (Ma)	Location	Reference
Acme *Operculodinium israelianum*	133–136	Early Pleistocene, MIS 95 (Unit N3b)	2.407–2.427	Netherlands, North Sea	Meijer et al., 2006; Noorbergen et al., 2015
Acme *Impagidinium multiplexum*	150	Early Pleistocene, MIS 97 (Unit N2b)	2.452–2.477	Netherlands, North Sea	Meijer et al., 2006; Noorbergen et al., 2015
LOD *Barssidinium* spp.	157	Late Pliocene	2.58	Netherlands, North Sea	Kuhlmann et al., 2006
LOD *Barssidinium pliocenicum*[a]	190	Late Pliocene	2.58	Netherlands, North Sea	Kuhlmann et al., 2006
			2.6	Eastern North Atlantic, DSDP 610A	De Schepper and Head, 2008, 2009
LOD *Operculodinium? eirikianum*[b]	201	Late Pliocene	2.6	Eastern North Atlantic, DSDP 610A	De Schepper and Head, 2008, 2009
			3.0	Norwegian Sea, ODP 642B	De Schepper et al., 2015, 2017
LOD *Invertocysta lacrymosa*[c]	265	Late Pliocene	2.72–2.74	Eastern North Atlantic, DSDP 610A	De Schepper and Head, 2008, 2009
		Mid Pliocene	3.27	Norwegian Sea, ODP 642B	De Schepper et al., 2015, 2017
LOD *Melitasphaeridium choanophorum*[d]	330	Late Pliocene	3.0	Eastern North Atlantic, DSDP 610A	De Schepper and Head, 2008, 2009
		Mid Pliocene	3.3	Norwegian Sea, ODP 642B	De Schepper et al., 2015, 2017
LOD *Operculodinium tegillatum*[e]	340	Early Pliocene	3.71	Eastern North Atlantic, DSDP 610A	De Schepper and Head, 2008, 2009
			4.6	Norwegian Sea, DSDP 642B	De Schepper et al., 2015, 2017
LOD *Reticulatosphaera actinocoronata*[f]	355	Early Pliocene	*ca.* 4.4	Northern North Atlantic, DSDP Site 611	Mudie, 1987; Baldauf et al., 1987
			4.64	Norwegian Sea, DSDP 642B	De Schepper et al., 2015, 2017

[a] Despite several reports on younger occurrences than 2.6 Ma outside the Dutch part of the North Sea for the genus *Barssidinium*, there is consistent evidence from multiple Dutch wells to maintain the magnetostratigraphically calibrated Gauss/Matuyama boundary (Kuhlmann et al., 2006). The dating is verified by the occurrences in the eastern North Atlantic (De Schepper and Head, 2009).

[b] The higher occurrence of *Operculodinium? eirikianum* is reported in ODP 642B at 3.0 Ma (De Schepper et al., 2015, 2017) and in the North Atlantic at 2.6 Ma (De Schepper and Head, 2008, 2009).

[c] The higher occurrence of *Invertocysta lacrymosa* is reported for the North Atlantic at 2.72–2.74 Ma (De Schepper and Head, 2008, 2009) and in the Norwegian Sea at 3.27 Ma (De Schepper et al., 2015, 2017). The former age of the event was followed in Belgium (Louwye and De Schepper, 2010).

[d] For the North Sea area, the LOD of *Melitasphaeridium choanophorum* was indicated at 3.6 Ma (Dybkjaer and Piasecki, 2010; Kuhlmann et al., 2006). The age assessment for the Danish sector of the North Sea is likely too old (De Schepper et al., 2017). In the Norwegian Sea the event is magnetostratigraphically calibrated to 3.27 Ma (De Schepper et al., 2017). In DSDP Site 610 the highest persistence occurrence of this taxon goes up to 3.0 Ma (De Schepper and Head, 2008).

[e] The LOD of *Operculodinium tegillatum* is recorded in the Nordic Seas at ca. 4.6 Ma (De Schepper et al., 2015, 2017) and in the North Atlantic at 3.71 Ma (De Schepper and Head, 2008, 2009). The latter age is followed in the North Sea at 3.71 Ma (Louwye and De Schepper, 2010).

[f] The LOD of *Reticulosphaera actinocoronata* at 4.64 Ma in the Norwegian Sea and at 4.45 Ma in the Iceland Sea corresponds to the well-established North Atlantic, including the North Sea area at 4.4–4.5 Ma (Louwye et al., 2004; Schreck et al., 2012; De Schepper et al., 2015, 2017).

The weighted average number of cyclopentane rings in tetramethylated brGDGTs (#Rings$_{tetra}$) was calculated cf. Sinninghe Damsté (2016):

$$\#\text{Rings}_{\text{tetra}} = \frac{[\text{Ib}] + 2 * [\text{Ic}]}{[\text{Ia}] + [\text{Ib}] + [\text{Ic}]} \quad (4)$$

2.6. Statistical analysis

To identify changes in the brGDGT assemblage and to assess variability in the brGDGT pool, principal component analysis (PCA) was performed with the software package SigmaPlot (Systat Software). Standardized fractional abundances of the major brGDGTs (excluding brGDGTs IIIb, IIIb′, IIIc and IIIc′) were used.

3. Results

3.1. Lithology and age model

The studied core section (404–136 m) consists of three formations, the Maassluis (157–136 m), the Oosterhout (333–157 m), and the Breda (404–333 m). The presence of marine dinocysts preferring outer neritic conditions (e.g. *Spiniferites*, *Operculodinium? eirikianum*) and bisaccates in common values (approx. 32% of the total sum of dinoflagellate cysts and sporomorphs) suggests an open-marine offshore conditions of the Hank site at the time of deposition of the Breda Fm. The Oosterhout Fm. sediments (333–157 m) consist almost exclusively of sands, except for one clay interval between 291–271 m. The sands deposited above the clay layer (271–157 m) contain abundant shells, suggesting that the shore was closer to the Hank site during this period. The overlying Maassluis Fm. (157–136 m) mostly consists of silt deposits interspersed with thin clay and sand deposits. The emergence of freshwater algae species (e.g. *Pediastrum*) and organisms preferring brackish water conditions (*Botryococcus*) in this section indicates a development towards estuarine conditions. Thus, the shore gradually moved closer to the Hank site over the evolution of the Pliocene and early Pleistocene. Eventually, the core site attained a deltaic character. This is also reflected in the age-depth model (Fig. 3), where the observed sedimentation rate increases drastically just before the Plio–Pleistocene transition at approximately 200 m.

The Pliocene–Pleistocene transition (∼154 m) is indicated by the increased proportion of cold-tolerant taxa such as *Habibacysta tectata* (Head et al., 1989; Jimenez-Moreno et al., 2006; Hennissen et al., 2017). Also, markers for the Piacenzian, (including taxa preferring relatively warmer conditions – like *Barssidinium pliocenicum, Invertocysta lacrymosa*, and *Melitasphaeridium choanophorum*) are absent above this depth.

The presence of hiatuses in the Hank core is unknown, however, the mixing of samples due to the core collection method leads to the smoothing out of hiatuses, if present. Thus, linear interpola-

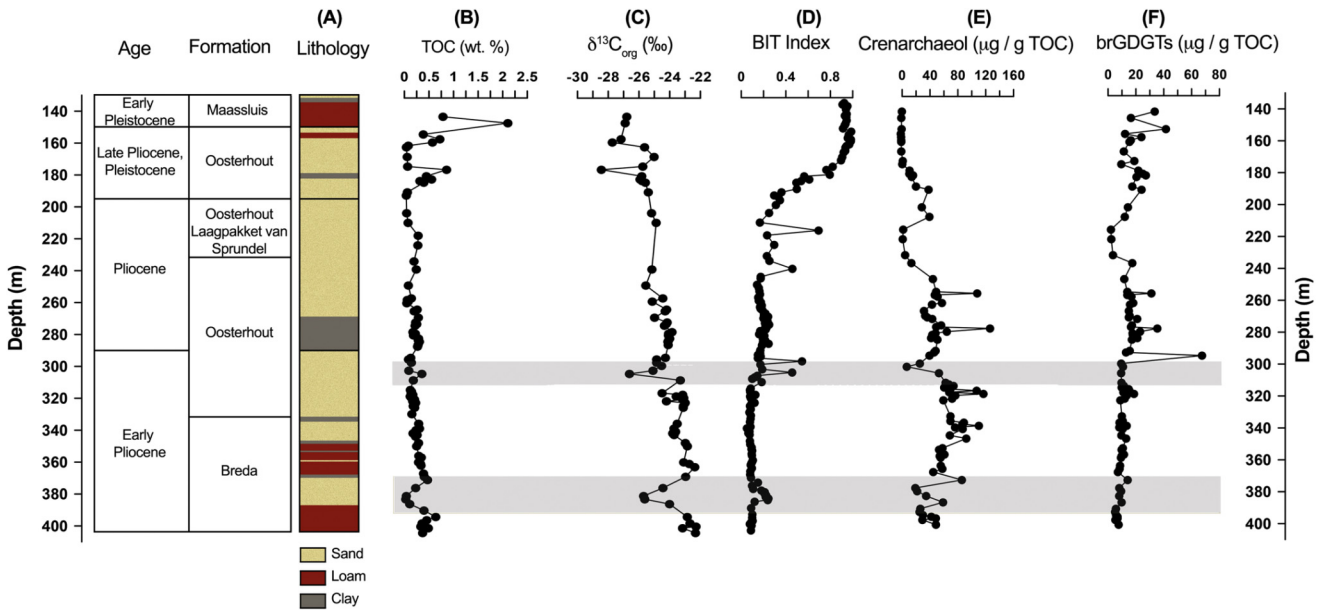

Fig. 4. Depth, age, and formation of the Hank sediments plotted with: (A) Lithology, (B) TOC content, (C) $\delta^{13}C_{org}$, (D) BIT index, (E) Crenarchaeol concentration (normalized against TOC), and (F) brGDGT concentration (normalized against TOC). The brGDGT concentrations represent the sum of all brGDGTs measured (Ia-IIIc′). The two shaded intervals represent Pliocene events discussed in the text.

tion between the age tie-points is used to estimate the age of the Hank sediments (Fig. 3). The obtained age model indicates that the studied interval encompasses the Early Pliocene (Zanclean) to the early Pleistocene (Gelasian), although the coastal setting suggests that the sedimentation rate may not always have been constant between tie-points at this site.

3.2. Bulk properties of organic material in the Hank Core

TOC content ranges from 0.02 to 2.1 wt.% (Fig. 4B), where TOC is lower in the Pliocene (>161 m; 0.25 wt.% on average) than in the Pleistocene part of the core (average 0.92 wt.%). The lowest TOC values (0.02–0.09 wt.%) occur in four intervals: 386–381 m, 261–259 m, 211–192 m, and 176–163 m (Fig. 4B). In general, TOC content follows the lithology, with the lowest TOC values corresponding to the sand intervals (0.02–0.81 wt.%), the highest values in the loam intervals (0.26–1.95 wt.%), and the clay layers possessing intermediate TOC values (0.19–0.54 wt.%).

The $\delta^{13}C_{org}$ values vary between −28.4 and −22.2‰, and show an overall decreasing trend from the Pliocene towards the Pleistocene, except during two distinct intervals in the Pliocene at 386–376 m and 305–300 m, which show more depleted $\delta^{13}C_{org}$ values ($\Delta\delta^{13}C_{org}$ ~3‰; shaded in Fig. 4C).

3.3. GDGT concentrations and proxies

Crenarchaeol and brGDGTs are present in all 155 samples analyzed, although brGDGTs IIIb, IIIb′, IIIc, and IIIc′ were below the detection limit in 47 samples. Crenarchaeol and total brGDGT concentrations are normalized to TOC to enable comparison of the abundances of the compounds, regardless of changes in lithology. The concentration of crenarchaeol varies between 0.2–130 $\mu g\,g^{-1}$ TOC, and shows a marked decrease starting in the Late Pliocene (190 m; Fig. 4E). The summed concentration of all brGDGTs varies between 1.5–67 $\mu g\,g^{-1}$ TOC, and brGDGTs generally occur in higher concentration from the Late Pliocene onwards (<200 m, Fig. 4F), apart from one spike in the record (~300 m). As a result, values for the BIT index are generally low (<0.2) in the Pliocene, apart from two intervals where the values of the BIT index increase to ~0.25–0.5 (386–376 and 305–300 m; shaded intervals, Fig. 4D). BIT index values then increase to a maximum of 0.98 ± 0.02 for Pleistocene sediments.

4. Discussion

4.1. Provenance of organic matter in the North Sea Sediments

During the Mid-Miocene, sediment supply to the North Sea basin was primarily dominated by the Eridanos river system, which drained the Fennoscandia and the Baltic States (Gibbard and Lewin, 2016). In the late Miocene (Tortonian), the proto Rhine–Meuse river system emerged, which drained the low-lying topography of central Europe (Wong et al., 2007). Due to the close proximity of the Hank site to the proto Rhine–Meuse river system (Fig. 2), it is assumed that the terrestrial OM delivered to this part of the southern North Sea basin is mostly derived from that river system.

The higher $\delta^{13}C_{org}$ values (−22 to −24‰) in the Pliocene section indicate a primarily marine origin of the OM, with a relatively smaller input from terrestrial sources (Tyson, 1995). The trend towards more depleted $\delta^{13}C_{org}$ values of < −26‰ in the Pleistocene suggests that the prevailing source of OM to the sediment changes to a terrestrial origin (i.e. soil and/or higher plant OM; Tyson, 1995) in this interval (<200 m). In addition, OM produced in rivers during transport may also contribute to the sedimentary $\delta^{13}C_{org}$ signal. However, this contribution is hard to identify, as there is no vast difference in $\delta^{13}C_{org}$ values of soil OM vs. river-produced OM (Cloern et al., 2002). Nevertheless, the clear shift in OM provenance from marine to terrestrial occurring at a core depth of ca. 200 m combined with the age model and lithology provides evidence that the Hank site became more deltaic during this time. Furthermore, two distinct shifts in $\delta^{13}C_{org}$ in the Pliocene section of the record represent periods with increased terrestrial OM input. This can be explained by a temporary lowering of the sea level, leading to marine regression, thus rendering the Hank site location closer to shore during these intervals (Fig. 4C, shaded intervals). Higher BIT index values, as well as increased abundances in terrestrial palynomorphs during both intervals also indicate an increase in terrestrial OM input at this time. Finally, the lithology of the core supports the argument that the Hank site was shallow(er) in these two intervals due to the presence of sandy deposits.

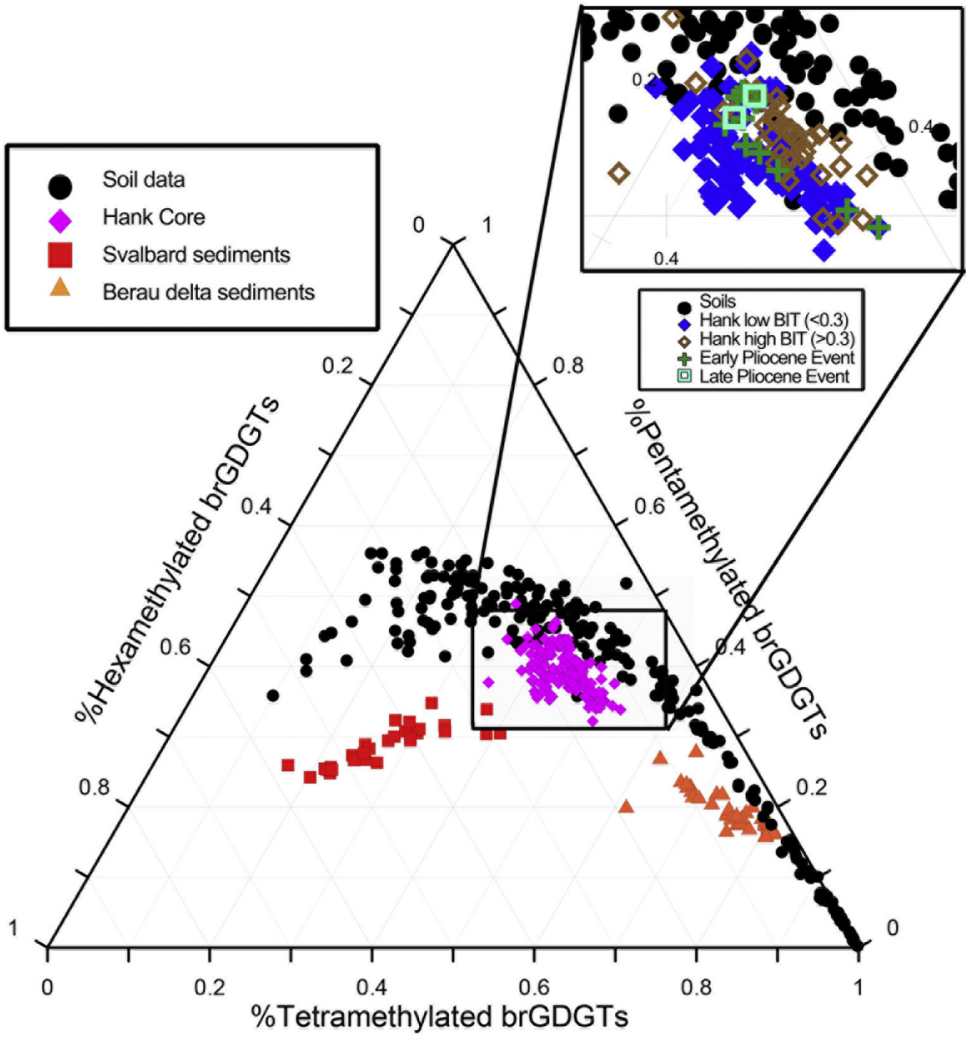

Fig. 5. Ternary diagram of the fractional abundances of the tetramethylated (% tetra), pentamethylated (% penta), and hexamethylated (% hexa) brGDGTs in the Hank core (magenta diamonds), the global soil calibration dataset (black circles), Svalbard fjord sediments (red squares), and the Berau Delta (orange triangles). The inset shows the Hank data separated into BIT index values >0.3 (brown open diamonds) and BIT index values <0.3 (dark blue closed diamonds) for comparison to the soil dataset. The two Pliocene events are indicated by green crosses (Early Pliocene event) and light blue open squares (Late Pliocene event). (For interpretation of the colors in the figure(s), the reader is referred to the web version of this article.)

Hence, periods of high BIT/low $\delta^{13}C_{org}$ values indicate that the shore was likely closer to the Hank site, as a result of a lower sea level related to an increase in global ice volume. This is similar to what has been observed for the Last Glacial Maximum in the Bay of Biscay, where high BIT indices were recorded during the sea-level low stand, which placed the paleo-coastline considerably closer to the site (Ménot et al., 2006). Due to the relatively low resolution of the current age model and the difficulties in making a straightforward benthic $\delta^{18}O$ record for shallow, coastal locations, we cannot directly assign the shaded intervals to specific events. From this point, the lower interval (385–375 m) is referred to as the 'Early Pliocene Event', and the upper interval (320–300 m) is referred to as the 'Late Pliocene Event'. Given the absence of indicators to suggest that the Miocene is reached at the base of the succession, the Early Pliocene Event occurs between 5.33–4.4 Ma. The age model also indicates that the Late Pliocene Event occurs between ~3.6–2.7 Ma. The large shift and leveling off of the BIT index and $\delta^{13}C_{org}$ records starting at 200 m likely reflects the onset of the NH glaciations that mark the Pleistocene (~2.6 Ma). The large increase in ice volume on the NH led to significant sea level lowering (Lisiecki and Raymo, 2005), which stranded the Hank site and consequently removed marine influence on the site.

4.2. Identifying sources of brGDGTs in the North Sea Basin

The covarying BIT and $\delta^{13}C_{org}$ records, and the recent findings on the in-situ production of brGDGTs in marine systems indicate the possibility of a mixed terrestrial and marine contribution of brGDGTs to the sediments (Peterse et al., 2009; De Jonge et al., 2014b; Sinninghe Damsté, 2016). It is likely that the processes governing the distribution of brGDGTs produced in marine systems differ from those in soils, and that temperatures derived from brGDGTs in marine sediments may not capture the MAT of the surrounding catchment. It is therefore essential to identify the contribution of marine-produced brGDGTs and to correct for their influence on the MAT record.

As a first step in assessing the sources of brGDGTs, the fractional abundances of the North Sea Basin brGDGTs are plotted in a ternary diagram and compared with data from the global soil calibration set (De Jonge et al., 2014a), following the approach of Sinninghe Damsté (2016). This shows that the fractional abundances of the North Sea Basin brGDGTs plot offset from the soils (Fig. 5), suggesting a marine brGDGT contribution to North Sea Basin sediments. However, comparison of these data with brGDGT data from the two coastal marine locations that have been analyzed with the improved chromatography method

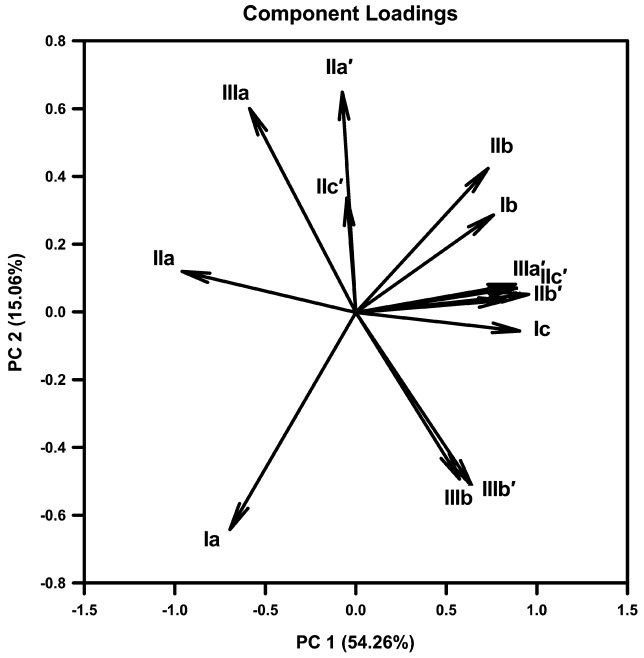

Fig. 6. PCA analysis based on fractional abundances of all 15 brGDGTs of the Hank core sediments. Species scores of the 15 brGDGTs on the first two PCs. Roman numerals refer to the structures from Fig. 1.

so far, i.e. Svalbard fjords and the Berau River delta, Indonesia (Sinninghe Damsté, 2016), indicates that the offset from the soil data is relatively small (Fig. 5). In comparison with the Svalbard and Berau sites, for which in situ production of brGDGTs has been suggested to be the predominant source (Peterse et al., 2009; Sinninghe Damsté, 2016), brGDGTs from the coastal North Sea appear to be mostly soil-derived. When considering the data in more detail, sediments with BIT index values >0.3 plot closer to the soil data than those with BIT index values <0.3 (Fig. 5). Also, the Pliocene sediments with higher BIT index values (Fig. 4, shaded intervals) plot closer to the soil data (Fig. 5). This is in good agreement with our earlier interpretation that higher values of the BIT index and depleted $\delta^{13}C_{org}$ reflect increased input of terrestrial OM, including soil-derived brGDGTs. Nevertheless, it also indicates that in sections with lower BIT index values marine in-situ production is probably modifying the brGDGT distribution.

To further elucidate trends in the downcore variations in brGDGT concentration and distribution, principal component analysis (PCA) was performed on the fractional abundances of the brGDGTs. Principal component PC1 described 54% of the variance in the dataset, whereas PC2 describes 15% (Fig. 6). The acyclic 5-methyl brGDGTs Ia, IIa, and IIIa all score negatively on PC1, whereas all cyclic brGDGTs score positively (Fig. 6). This indicates a distinct relationship between PC1 and the brGDGTs with cyclopentane moieties. Indeed, when the $\#rings_{tetra}$ is compared to the PC1 scores, a strong positive correlation is observed ($r^2 = 0.75$).

The $\#rings_{tetra}$ has been found to vary from 0–0.7 in soils from the global soil calibration set (De Jonge et al., 2014a), but exceeds these values in coastal marine sediments with considerable in situ brGDGT production, likely because the pore waters of marine sediments are alkaline (Peterse et al., 2009; Sinninghe Damsté, 2016), and brGDGT production at higher pH tends to result in the production of higher relative amounts of cyclopentane-containing brGDGTs (Weijers et al., 2007a; Peterse et al., 2012). A contribution of marine in-situ produced brGDGTs to marine sediments in coast-shelf transects from the Berau Delta, East China Sea shelf system, and the Iberian margin was clearly reflected by zones where $\#rings_{tetra}$ >0.7, which was consequently proposed as an indicator value for coastal marine sediments that possess a primarily non-soil source input (Sinninghe Damsté, 2016). In the North Sea basin sediments, the $\#rings_{tetra}$ ranges from 0.20–0.59 (Fig. 7B). Although these values are within the range for soils in the global calibration set, soils with $\#rings_{tetra}$ >0.4 are mostly alkaline soils (pH > 7), often occurring in arid deserts (De Jonge et al., 2014a). The majority of the soils in the catchment area of the Hank site are unlikely to be alkaline in nature (Reuter et al., 2008), and the average soil pH value for soils in North Western Europe is 6.5 (global soil dataset, excluding Sweden, Ireland, Norway, and Scotland, De Jonge et al., 2014a). Thus, the fact that $\#rings_{tetra}$ exceeds 0.4 for parts of the record more likely implies that the brGDGT distribution in these intervals has a marine overprint. However, as the Hank $\#rings_{tetra}$ record is consistently <0.7, a substantial proportion of brGDGTs is soil-derived, particularly for the Pleistocene sediments (average $\#rings_{tetra}$ ~0.3; Fig. 7B). Furthermore, $\#rings_{tetra}$ generally increases with depth, where higher values particularly in the Pliocene sediments suggest that there may be a contribution of marine produced brGDGTs (Fig. 7B).

It is apparent that the PC1 varies in concert with $\#rings_{tetra}$ over depth, and they both follow the patterns of the BIT index and $\delta^{13}C_{org}$ records: all Pleistocene samples scoring positively on PC1, and the majority of Pliocene samples scoring negatively (Fig. 7B,C). Indeed, in a cross plot of BIT index vs. $\#rings_{tetra}$ ($r^2 = 0.68$; Fig. 8), the depths with high BIT index (>0.9) occurring in the Pleistocene have $\#rings_{tetra}$ between ~0.25–0.3, typical values for acidic soils. Furthermore, the two intervals with increased terrestrial input recognized in the BIT index and $\delta^{13}C_{org}$ records (Fig. 4C,D) have positive values on PC1. The covariance of the BIT index, $\delta^{13}C_{org}$, $\#rings_{tetra}$ and PC1 records indicates that the variation in marine and terrestrial brGDGT contribution to the North Sea sediments is the dominant factor determining the variance in the dataset. This suggests that in the Hank sediments, a more negative score on PC1 and a higher $\#rings_{tetra}$ can be used as indicators of marine in situ brGDGT production.

Consequently, we applied the $\#rings_{tetra}$ record to disentangle the marine and terrestrial sources of the brGDGTs in the North Sea basin using two end-member modeling. A soil end-member value of $\#rings_{tetra} = 0.29$ was chosen based on the $\#rings_{tetra}$ for the sediments with highest soil input (BIT index >0.9) under the assumption that pH of the soils in the hinterland did not change substantially over the period studied. The samples chosen for the soil end-member ($n = 23$) all occur in the late Pliocene/early Pleistocene interval of the core, during which mean annual precipitation (MAP, a controlling factor for soil pH) in the Lower Rhine Basin did not change significantly (1000 mm/yr ±100; Mosbrugger et al., 2005). The marine end-member was set at 0.93, based on the $\#rings_{tetra}$ in the marine sediments from Svalbard, where the brGDGT distribution represents almost exclusively marine in-situ production (Peterse et al., 2009; Sinninghe Damsté, 2016). Using these end-members, the $\#rings_{tetra}$ record was translated into a record indicating the relative contributions of soil vs. marine brGDGTs (Fig. 7D). This record indicates on average ~35% marine contribution during the Pliocene, and ~0–27% during the Pleistocene. The two Pliocene intervals with presumed lower sea level and increased terrestrial input (shaded intervals, Figs. 4 and 7) are also characterized by a lower contribution of marine brGDGTs ($\Delta_{terrestrial\text{-}marine}$ ~20%).

4.3. BrGDGT-based MAT reconstruction

Application of the latest soil transfer function of De Jonge et al. (2014a) to brGDGTs in the Hank core generates a record of MAT_{mr} reflecting a temperature range of 7–15 °C (Fig. 7E, orange line). Overall, MATs decrease steadily towards the Pleistocene, with additional notable cooler periods ($\Delta T = 3$–5 °C) corresponding with

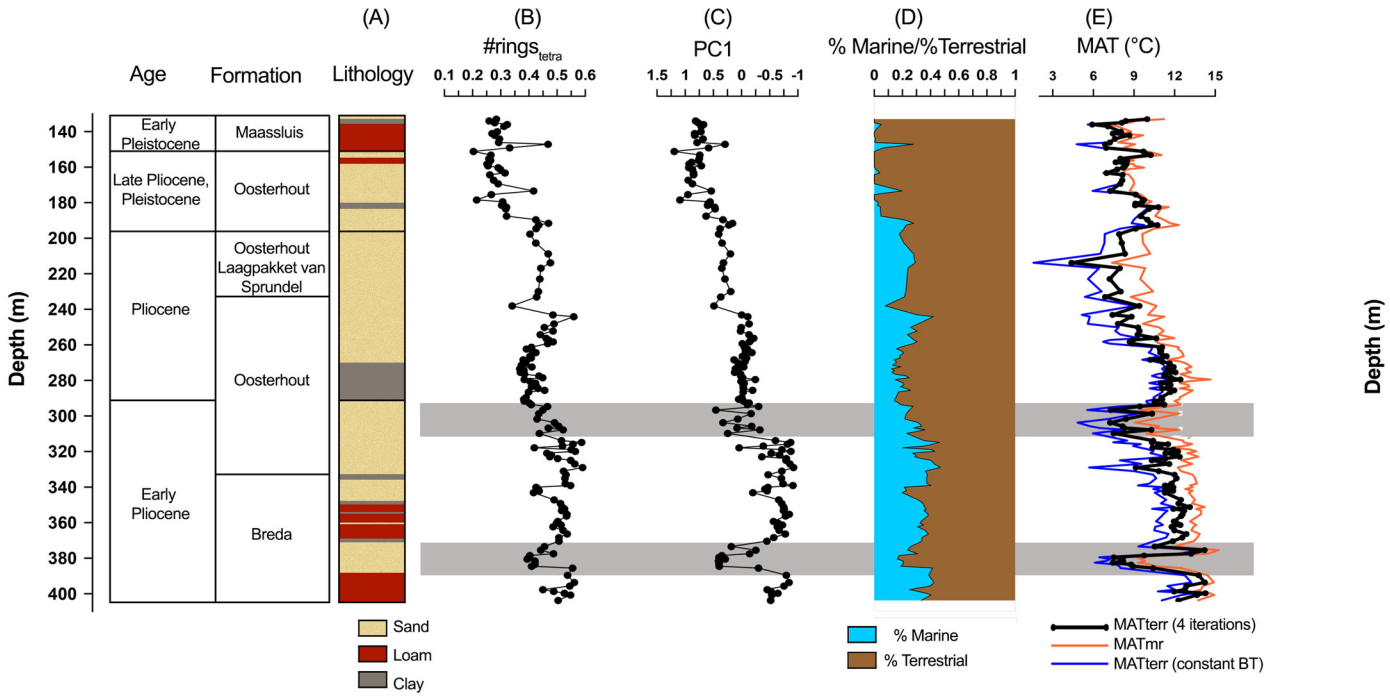

Fig. 7. Depth, age, and formation of the Hank sediments plotted with brGDGT proxies. (A) Lithology, (B) #rings$_{tetra}$, (C) PC1, (D) % Marine/% Terrestrial, and (E) MAT records (orange line for the MAT$_{mr}$ record, dark blue line for the MAT$_{terrestrial}$ calculated with constant bottom water temperature, and solid black line with circle symbols for the MAT$_{terrestrial}$ using the iteration method) of the Hank sediments are plotted against depth. The two shaded bars represent Pliocene events. (For interpretation of the colors in the figure(s), the reader is referred to the web version of this article.)

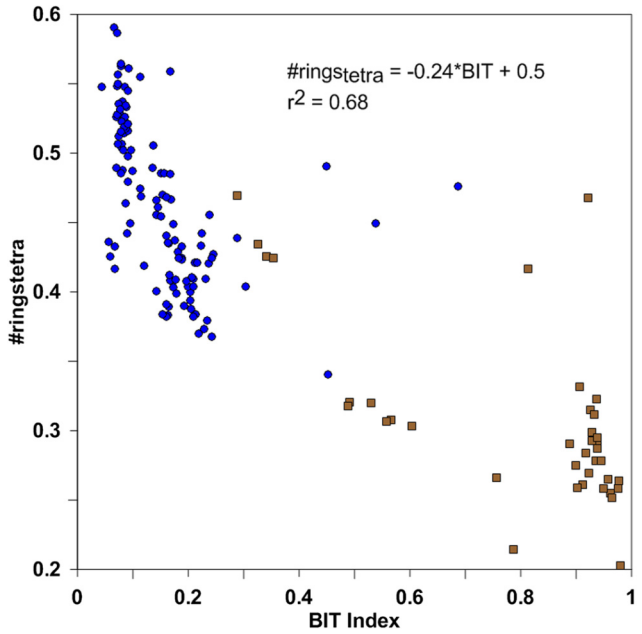

Fig. 8. #rings$_{tetra}$ values for Hank sediments plotted against corresponding BIT index values, with linear fit equation and coefficient of determination (r^2) shown. Samples plotted as blue circles occur at sediment core depths (>200 m) and samples plotted in brown squares occur at core depths (<200 m). (For interpretation of the colors in the figure(s), the reader is referred to the web version of this article.)

the Early and Late Pliocene events discussed earlier (shaded intervals; Fig. 7E). The period directly after the Late Pliocene event represents a warm period, which is connected with a thick clay interval in the lithology (300–280 m; Fig. 4A), pointing to a relatively higher sea level.

However, this MAT reconstruction is only valid if the brGDGTs are predominantly derived from soil, whereas the values of #rings$_{tetra}$ indicate that brGDGT sources to the North Sea basin vary throughout the record. Hence, to obtain the 'true' terrestrial MAT (MAT$_{terr}$) signal, the marine contribution to the brGDGT distribution must be removed from the MAT record. This can be achieved with the use of two transfer functions: one for soils, for which the recent MBT′5Me–MAT global soil calibration data set will be used (De Jonge et al., 2014a), and a second, new function reflecting in-situ production in coastal marine sediments. The MBT′5Me index for the Hank sediments represents a mix of the marine (MBT′5Me$_{marine}$) and terrestrial (MBT′5Me$_{terrestrial}$) inputs. Consequently, the MAT$_{terr}$ record can be obtained by subtracting the marine contribution to the 'mixed' MBT′5Me values.

The first step for this procedure is to create the function needed to transfer coastal marine brGDGT distributions to marine water temperatures, similar to the transfer function for the global soil calibration set of De Jonge et al. (2014a). In situ water temperatures are used instead of air temperatures, due to the fact that the temperature response of brGDGTs produced in the marine environment is more likely to record in situ water temperature rather than air temperature. So far, 'novel' brGDGT data (i.e. including the separate integration of 5- and 6-methyl brGDGT isomers) is only available for two coastal marine sites, i.e. Svalbard (Peterse et al., 2009) and the Berau delta (Sinninghe Damsté, 2016). Based upon the low BIT index values (<0.1) and high values of #rings$_{tetra}$ (>0.7), these authors concluded that the brGDGT distribution at these two sites is predominantly composed of in situ produced brGDGTs (Peterse et al., 2009; Sinninghe Damsté, 2016).

Although the number of global sites is limited, they conveniently represent a polar and tropical environment, stretching the reach of the temperature range, thus preventing extrapolation of the regression line. In addition, available brGDGT data from one surface sediment located in the Tagus drainage basin off the coast of Portugal was added (Warden et al., 2016). We supplemented this mid-latitude datapoint with surface sediments from the Portuguese margin (Zell et al., 2015), of which those characterized by a low BIT index (<0.1) and a high value of #rings$_{tetra}$ (>0.7) were

reanalyzed using the new chromatography method (Hopmans et al., 2016).

In order to formulate the regression model, MBT′5Me values from the Berau delta ($n = 11$), Svalbard ($n = 28$), Portuguese margin ($n = 9$) sites were plotted against in situ bottom water temperatures at the respective sites, reflecting the depth at which the surface sediments were obtained. It is therefore assumed that the MBT′5Me value represented by these three sites represents a 100% marine signal of brGDGT production. We use bottom water temperatures from ca. 40–90 m for the shallow Berau delta, 200–300 m for Svalbard, and 300–1000 m for the samples from the Portuguese margin (Peterse et al., 2009; Zell et al., 2015; Sinninghe Damsté, 2016).

The resulting linear regression fit produced the following coastal marine transfer function (Fig. 9):

$$\mathrm{BWT} = 59.5 * \mathrm{MBT'5Me_{marine}} - 23.7 \quad (R^2 = 0.95) \tag{5}$$

where BWT is the bottom water temperature. The marine transfer function possesses a slightly steeper slope than the soil calibration line (Fig. 9). This translates into larger changes in the high (MBT′5Me >0.7) and low (MBT′5Me <0.4) ends of the calibration compared to the soil calibration line.

Subsequently, the MBT′5Me index can be corrected for the contribution of marine brGDGTs by separating the terrestrial and marine contributions to the total brGDGT pool:

$$\mathrm{MBT'5Me_{total}} = \%\text{terrestrial brGDGTs} * \mathrm{MBT'5Me_{terrestrial}} + \%\text{marine brGDGTs} * \mathrm{MBT'5Me_{marine}} \tag{6}$$

where $\mathrm{MBT'5Me_{marine}}$ is described by Eq. (5), $\mathrm{MBT'5Me_{total}}$ is the index measured on the sediment samples, and the %marine and %terrestrial brGDGTs are calculated as described in section 4.2. To estimate $\mathrm{MBT'5Me_{marine}}$, a BWT must be chosen that reflects the bottom water temperature of the North Sea in the Pliocene. The current average BWT (11.5 °C) of the North Sea at 30 m depth is determined by the winter minimum of 6–7 °C and the summer maximum of 16–17 °C (Johnson et al., 2009; Boyer et al., 2013). During the Pliocene, ostracod assemblages in the Coralline Crag Formation in England, with an estimated paleodepth of greater than 50 m, suggest winter minimum and summer maximum seafloor temperatures of 11 and 18 °C, respectively (Hodgson and Funnel, 1987; Johnson et al., 2009). Using the average of the summer and winter Pliocene temperatures proposed by Johnson et al. (2009), we estimate the Pliocene BWT for the North Sea as 14.5 °C, i.e. ∼3 °C higher than present. The use of a constant BWT results in a constant $\mathrm{MBT'5Me_{marine}}$ value (0.64) that is used in Eq. (6) to correct $\mathrm{MBT'5Me_{total}}$. The measured $\mathrm{MBT'5Me_{total}}$ and constant $\mathrm{MBT'5Me_{marine}}$ values are then combined with the %Terrestrial/%Marine ratios to determine $\mathrm{MBT'5Me_{terrestrial}}$. The corrected temperature record is obtained by applying the soil transfer function for MAT and MBT′5Me, as described by De Jonge et al. (2014a; Fig. 7E, blue line):

$$\mathrm{MAT_{terr}} = 31.5 * \mathrm{MBT'5Me_{terrestrial}} - 8.6 \quad (R^2 = 0.66) \tag{7}$$

This calculation does not take into account the fact that the BWT is likely to change over time as a response to regional climate changes. As it is quite likely that the BWT of the coastal North Sea did change over the course of the Pliocene and the Pleistocene, we used the $\mathrm{MAT_{terr}}$ record generated to predict BWT in a series of iterations. The present day difference in temperature between the annual mean temperature of the bottom water of the North Sea (∼11.5 °C) and the MAT of the Netherlands (∼10 °C) was calculated ($\Delta T = 1.5$ °C; van Engelen et al., 2001; Boyer et al., 2013)

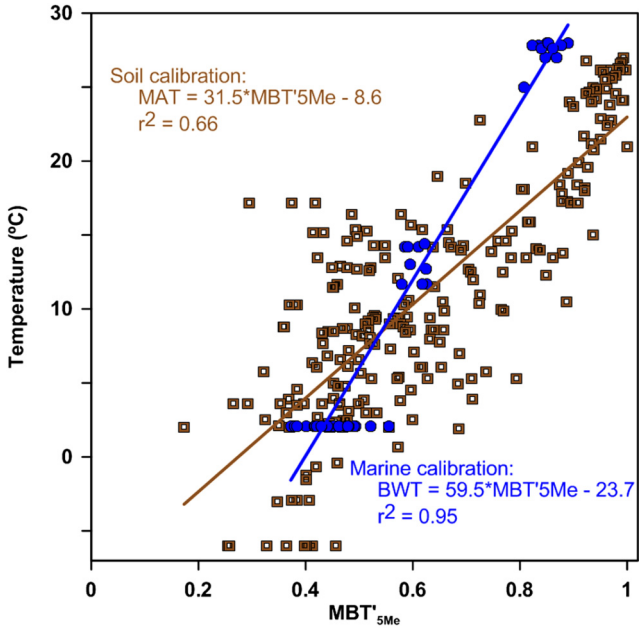

Fig. 9. Cross plot and regression lines for the MBT′5Me value versus measured MAT for the soil calibration data set (open brown squares) and versus BWT for the Svalbard (Peterse et al., 2009), Berau Delta (Sinninghe Damsté, 2016), and Portuguese margin sediments (reanalyzed from Zell et al., 2015; Warden et al., 2016; blue circles). (For interpretation of the colors in the figure(s), the reader is referred to the web version of this article.)

and this ΔT was assumed to also hold for the Pliocene and the Pleistocene. This allows calculating BWT from $\mathrm{MAT_{terr}}$ and feed newly calculated BWTs for each individual sediment horizon back into the calculation. Starting with a constant bottom water temperature of 14.5 °C a series of four iterations were performed after which the calculated $\mathrm{MAT_{terr}}$ for each individual sediment horizon did not change substantially (<0.6 °C) from its predecessor value. The corrected $\mathrm{MAT_{terr}}$ record (Fig. 7E, solid black line with circle symbols) varies between 4 and 14 °C, showing a distinctly lower range of temperatures ($\Delta T = 10$ °C) than the $\mathrm{MAT_{terr}}$ record using a constant BWT value ($\Delta T = 12$ °C; Fig. 7E). In both records the general cooling trend from older to younger sediments is evident.

A number of assumptions are made to arrive at the final $\mathrm{MAT_{terr}}$, some of which cannot be fully explored regarding the error they propagate through to the estimation of temperature. These include the assumptions i) that all terrestrial OM is derived from the Rhine–Meuse river system, and ii) that the MBT′5Me value of the three reference sites (Svalbard, Berau delta, and Portuguese margin) represents a 100% marine signal. Assumption i) would require a detailed study of the OM composition in the different river catchments that discharge into the North Sea Basin during the Pliocene, which is beyond the scope of this paper, and assumption ii) cannot be confirmed as long as the exact producer(s) of brGDGTs remain(s) unknown. The most important assumptions that can be addressed with regards to the error on reconstructed temperatures are iii) estimating the Pliocene BWT of the North Sea, and iv) the temperature difference between the continental and bottom water temperatures in the North Sea, ΔT. We explore the error in our estimate of Pliocene BWT by also carrying out the correction steps outlined above for a cooler (11.5 °C) and warmer (17.5 °C) BWT, which results in maximum deviations of −1.3 °C and 1.5 °C respectively. Secondly, we explore the error associated with slightly different values for ΔT by re-doing the iteration for a smaller (0.5 °C) and larger ΔT (3 °C). The errors associated with different ΔT maximize at −0.46 °C for a larger ΔT and 0.31 °C for a smaller ΔT. Taking all the errors associated with correcting the MAT record into account, shows that they fall well within the cal-

ibration error of the brGDGT temperature proxy (4.6 °C; De Jonge et al., 2014a). This calibration error reflects a systematic error most likely affecting calculated absolute temperatures in a similar way. Note that the timing, as well as the direction of the changes in the temperature record are not influenced by the assumptions made, and can thus be considered reliable.

4.4. Pliocene air temperature evolution in NW Europe

Our final, corrected continental temperature record (MAT_{terr}) retains the original pattern of the MAT_{mr} record, with higher temperatures in the Pliocene and a gradual cooling that is initiated in the Late Pliocene and carries on into the Early Pleistocene (Fig. 7E). This gradual cooling trend is in strong agreement with existing global climate records, for example the global benthic oxygen isotope stack (Lisiecki and Raymo, 2005). Hence, despite the large number of assumptions made in the correction of the temperature record, the method proposed here leads to encouraging results.

The MAT_{terr} record indicates that MAT was ~12–14 °C during the Early Pliocene (Fig. 7E), which matches well with the brGDGT-derived temperatures of 14 °C reported for South-eastern Netherlands during the same period (Donders et al., 2009; using the calibration of Weijers et al., 2007a). The temperatures also match those recorded in Central Europe, using an approach based on the occurrence of seeds, fruits, and leaf remnants in continental sedimentary records (13 °C; Mosbrugger et al., 2005).

The two colder (Δ 5–7 °C) periods in the Pliocene interval present in the initial MAT_{mr} record are retained in the MAT_{terr} record (shaded intervals, Fig. 7E). These two periods occur simultaneously with the Early Pliocene event and Late Pliocene event (shaded intervals, Fig. 4), which were associated with a lower sea level. Given this synchroneity, the timing of the Early and Late Pliocene events fit the framework for Pliocene glaciations composed by De Schepper et al. (2014). The authors identified a Pliocene glacial at 4 Ma (Fronval and Jansen, 1996; St John and Krissek, 2002; De Schepper et al., 2014), which could correspond with the occurrence of the Early Pliocene event in our record. Our multi-proxy records thus support the existence of (a) glaciation(s) during the early Pliocene (De Schepper et al., 2014), and provide the first evidence that the influence of the early Pliocene glaciations on the Northern Hemisphere reached into the North-western European continent.

Furthermore, we also tentatively link the Late Pliocene event with either the Pliocene glacial at 3.6 Ma (De Schepper et al., 2014), or the well-documented M2 glacial (Lisiecki and Raymo, 2005; Mudelsee and Raymo, 2005; Naish and Wilson, 2009). The depth and age of the Late Pliocene event indicates a substantial cool event lasting significantly longer than the M2 event (3312–3264 ka), such that this glacial might be combination of two or more glacials in this record (possibly the 3.6 Ma glacial and the M2; De Schepper et al., 2014). The amplitude of the cooling of the late Pliocene glacial(s) (ΔT ~4 °C) is comparable to that of ~3–6 °C for the M2 glaciation recorded by alkenone- and Mg/Ca-derived SSTs at DSDP site 610 and IODP site U1308 in the North Atlantic (De Schepper et al., 2013), as well as with that reflected by pollen assemblages from Lake Elgygytgyn in NE Russia (Brigham-Grette et al., 2013). Alkenone SST records of the M2 glaciation in a tropical SST stack show lower amplitudes of 2.5 °C (Herbert et al., 2010), so the MAT_{terr} record at this North Western European location also supports the interpretation of a greater latitudinal temperature gradient during the Pliocene.

We speculate that the MPWP is represented by the interval of 295–263 m, and occurs directly after the Late Pliocene Glacial. The interval associated with the MPWP is characterized by sustained elevated MATs (10.5–12.0 °C; Fig. 7E). When absolute temperatures are compared with the present MAT in NW Europe (~9.5 °C), they largely match the global MPWP temperature estimates of 2–3 °C warmer than the present day determined by the PRISM group (Dowsett et al., 2012). The warmer climate is also reflected in the BIT index, $\delta^{13}C_{org}$, and lithology records, which indicate a larger marine influence at the study location. MATs are furthermore comparable with MPWP temperature estimates based on pollen spectra from the Lower Rhine Basin (14.1 ± 0.2 °C, 3.6–2.6 Ma; Utescher et al., 2000), Germany (13.9 ± 0.5 °C, 3.2–2.6 Ma; Uhl et al., 2007), and south-east England (12.8 ± 1.3 °C, 3–2.6 Ma; Head, 1998). The HadAM3 GCM model for the mid-Pliocene (Pope et al., 2000; Haywood et al., 2002) produces a temperature estimate of 13.8 ± 0.4 °C for the region of west Germany (Salzmann et al., 2008), which is slightly higher than reflected by the brGDGTs at Hank. All current paleodata (including the Hank MAT_{terr} record) suggest that the climate in Northwestern Europe was approximately 2–6 °C warmer than present in the Pliocene.

Following the Plio–Pleistocene transition, MATs decrease, coinciding with an increase in BIT index values and depletion in $\delta^{13}C_{org}$. The high amplitude temperature variations ($\Delta T = 5$ °C) indicate the onset of the glacial–interglacial cycles of the Pleistocene (Raymo et al., 2006). Temperatures in this section of the record (6–11 °C) lie in the median between the reconstructed pollen-based mean temperature of coldest and warmest month (MTC and MTW) estimates for the Netherlands during the Tiglian (~0 and ~18 °C, respectively; Zagwijn, 1963; Pross and Klotz, 2002).

5. Conclusions

Bulk OM and brGDGT data in a sediment core from the North Sea basin indicates that the average number of cyclopentane rings ($\#rings_{tetra}$) can be used to identify and disentangle the provenance of brGDGTs in coastal marine sediments. Subsequent use of a newly developed coastal marine brGDGT temperature calibration and end member modeling can improve the reliability of brGDGT-based MAT reconstructions by correcting for marine contributions to the brGDGT pool in these settings. Applying these correction steps to the Pliocene section of the sediment core leads to a continental record (MAT_{terr}) of Pliocene temperature evolution in North Western Europe. The MAT_{terr} record indicates that NW Europe was approximately 1–2 °C warmer than present during the MPWP. Furthermore, the influence of two early Pliocene glaciations could be identified. The occurrence of these early Pliocene glaciations is supported by a simultaneous increase in BIT index value and a decrease (2–3‰) in $\delta^{13}C_{org}$ values, likely caused by sea level lowering due to waxing ice sheets on the NH. The good fit of our corrected MAT_{terr} record with existing global climate records indicates the promise of our method to resolve the influence of mixed brGDGT sources in coastal marine sediments on continental MAT reconstruction. Before the correction method can be widely applied, additional brGDGT data from coastal shelf environments is needed to strengthen the coastal marine brGDGT temperature calibration. This is currently hampered by to the limited number of studies that measure the 5- and 6-methyl brGDGTs separately in these specific settings.

Acknowledgements

We like to thank Dr. Stijn De Schepper and an anonymous reviewer for their comments, which greatly helped to improve this manuscript. The authors thank Natasja Welters and Arnold van Dijk for assistance with TOC and $\delta^{13}C_{org}$ analyses, and Denise Dorhout for re-analysis of the Portuguese margin samples. The work was supported by funding from the Netherlands Earth System Science Center (NESSC) through a gravitation grant (NWO 024.002.001) from the Dutch Ministry for Education, Culture and Science to

JSSD. NWO grant #834.11.006 enabled the purchase of the UHPLC-MS system used for GDGT analyses.

References

Baldauf, J.G., Thomas, E., Clement, B., Takayama, T., Weaver, P.P.E., Backman, J., Jenkins, G., Mudie, P.J., Westbergsmith, M., 1987. Magnetostratigraphic and biostratigraphic synthesis, Deep-Sea Drilling Project LEG-94. Init. Rep. Deep Sea Drill. Project 94, 1159–1205.

Boyer, T.P., Antonov, J.I., Baranova, O.K., Coleman, C., Garcia, H.E., Grodsky, A., Johnson, D.R., Locarnini, R.A., Mishonov, A.V., O'Brien, T.D., Paver, C.R., Reagan, J.R., Seidov, D., Smolyar, I.V., Zweng, M.M., 2013. World ocean database 2013. In: Levitus, S. (Ed.), NOAA Atlas NESDIS 72. Mishonov, A. (Technical Ed.). Silver Spring, MD. 209 pp. https://doi.org/10.7289/V5NZ85MT.

Brigham-Grette, J., Melles, M., Minyuk, P., Andreev, A., Tarasov, P., DeConto, R., Koenig, S., Nowaczyk, N., Wennrich, V., Rosén, P., Haltia, E., 2013. Pliocene warmth, polar amplification, and stepped Pleistocene cooling recorded in NE Arctic Russia. Science 340 (6139), 1421–1427. https://doi.org/10.1126/science.1233137.

Cloern, J.E., Canuel, E.A., Harris, D., 2002. Stable carbon and nitrogen isotope composition of aquatic and terrestrial plants of the San Francisco Bay estuarine system. Limnol. Oceanogr. 47, 713–729. https://doi.org/10.4319/lo.2002.47.3.0713.

De Jonge, C., Hopmans, E.C., Stadnitskaia, A., Rijpstra, W.I.C., Hofland, R., Tegelaar, E., Sinninghe Damsté, J.S., 2013. Identification of novel penta- and hexamethylated branched glycerol dialkyl glycerol tetraethers in peat using HPLC-MS 2, GC-MS and GC-SMB-MS. Org. Geochem. 54, 78–82. https://doi.org/10.1016/j.orggeochem.2012.10.004.

De Jonge, C., Hopmans, E.C., Zell, C.I., Kim, J.H., Schouten, S., Sinninghe Damsté, J.S., 2014a. Occurrence and abundance of 6-methyl branched glycerol dialkyl glycerol tetraethers in soils: implications for palaeoclimate reconstruction. Geochim. Cosmochim. Acta 141, 97–112. https://doi.org/10.1016/j.gca.2014.06.013.

De Jonge, C., Stadnitskaia, A., Hopmans, E.C., Cherkashov, G., Fedotov, A., Sinninghe Damsté, J.S., 2014b. In situ produced branched glycerol dialkyl glycerol tetraethers in suspended particulate matter from the Yenisei River, Eastern Siberia. Geochim. Cosmochim. Acta 125, 476–491. https://doi.org/10.1016/j.gca.2013.10.031.

De Jonge, C., Stadnitskaia, A., Hopmans, E.C., Cherkashov, G., Fedotov, A., Streletskaya, I.D., Vasiliev, A.A., Sinninghe Damsté, J.S., 2015. Drastic changes in the distribution of branched tetraether lipids in suspended matter and sediments from the Yenisei River and Kara Sea (Siberia): implications for the use of brGDGT-based proxies in coastal marine sediments. Geochim. Cosmochim. Acta 165, 200–225. https://doi.org/10.1016/j.gca.2015.05.044.

De Schepper, S., Head, M.J., 2008. Age calibration of dinoflagellate cyst and acritarch events in the Pliocene–Pleistocene of the eastern North Atlantic (DSDP Hole 610A). Stratigraphy 5 (2), 137–161.

De Schepper, S., Head, M.J., 2009. Pliocene and Pleistocene dinoflagellate cyst and acritarch zonation of DSDP Hole 610A, eastern North Atlantic. Palynology 33, 179–218.

De Schepper, S., Groeneveld, J., Naafs, B.D.A., Van Renterghem, C., Hennissen, J., Head, M.J., Louwye, S., Fabian, K., 2013. Northern hemisphere glaciation during the globally warm early late Pliocene. PLoS ONE 8, e81508.

De Schepper, S., Gibbard, P.L., Salzmann, U., Ehlers, J., 2014. A global synthesis of the marine and terrestrial evidence for glaciation during the Pliocene Epoch. Earth-Sci. Rev. 135, 83–102. https://doi.org/10.1016/j.earscirev.2014.04.003.

De Schepper, S., Schreck, M., Beck, K.M., Matthiessen, J., Fahl, K., Mangerud, G., 2015. Early Pliocene onset of modern Nordic Seas circulation related to ocean gateway changes. Nat. Commun. 6. https://doi.org/10.1038/ncomms9659.

De Schepper, S., Beck, K.M., Mangerud, G., 2017. Late Neogene dinoflagellate cyst and acritarch biostratigraphy for Ocean Drilling Program Hole 642B, Norwegian Sea. Rev. Palaeobot. Palynol. 236, 12–32. https://doi.org/10.1016/j.revpalbo.2016.08.005.

De Wet, G.A., Castañeda, I.S., DeConto, R.M., Brigham-Grette, J., 2016. A high-resolution mid-Pleistocene temperature record from Arctic Lake El'gygytgyn: a 50 kyr super interglacial from MIS 33 to MIS 31? Earth Planet. Sci. Lett. 436, 56–63. https://doi.org/10.1016/j.epsl.2015.12.021.

Donders, T.H., Weijers, J.W.H., Munsterman, D.K., Kloosterboer-van Hoeve, M.L., Buckles, L.K., Pancost, R.D., Schouten, S., Sinninghe Damsté, J.S., Brinkhuis, H., 2009. Strong climate coupling of terrestrial and marine environments in the Miocene of northwest Europe. Earth Planet. Sci. Lett. 281, 215–225. https://doi.org/10.1016/j.epsl.2009.02.034.

Dowsett, H., Thompson, R., Barron, J., Cronin, T., Fleming, F., Ishman, S., Poore, R., Willard, D., Holtz Jr, T., 1994. Joint investigations of the Middle Pliocene climate, I: PRISM paleoenvironmental reconstructions. Glob. Planet. Change 9 (3–4), 169–195. https://doi.org/10.1016/0921-8181(94)90015-9.

Dowsett, H.J., Robinson, M.M., Haywood, A.M., Salzmann, U., Hill, D.J., Sohl, L.E., Chandler, M., Williams, M., Foley, K., Stoll, D.K., 2010. The PRISM3D paleoenvironmental reconstruction. Stratigraphy 7, 123–139.

Dowsett, H.J., Robinson, M.M., Haywood, A.M., Hill, D.J., Dolan, A.M., Stoll, D.K., Abe-Ouchi, A., Chandler, M.A., Rosenbloom, N.A., Otto-Bliesner, B.L., Bragg, F.J., 2012. Assessing confidence in Pliocene sea surface temperatures to evaluate predictive models. Nat. Clim. Change 2, 365–371. https://doi.org/10.1038/nclimate1455.

Dybkjaer, K., Piasecki, S., 2010. Neogene dinocyst zonation for the eastern North Sea Basin, Denmark. Rev. Palaeobot. Palynol. 161, 1–29. https://doi.org/10.1016/j.revpalbo.2010.02.005.

Fronval, T., Jansen, E., 1996. Late Neogene paleoclimates and paleoceanography in the Iceland–Norwegian Sea: evidence from the Iceland and Vøring Plateaus. Proc. Ocean Drill. Program Sci. Results 151, 455–468.

Gibbard, P.L., Lewin, J., 2003. The history of the major rivers of southern Britain during the Tertiary. J. Geol. Soc. 160 (6), 829–845. https://doi.org/10.1144/0016-764902-137.

Gibbard, P.L., Lewin, J., 2016. Filling the North Sea Basin: cenozoic sediment sources and river styles (André Dumont medallist lecture 2014). Geol. Belg. 19, 201–217.

Haywood, A.M., Valdes, P.J., Francis, J.E., Sellwood, B.W., 2002. Global middle Pliocene biome reconstruction: a data/model synthesis. Geochem. Geophys. Geosyst. 3 (12), 1–18. https://doi.org/10.1029/2002GC000358.

Haywood, A.M., Dowsett, H.J., Dolan, A.M., 2016a. Integrating geological archives and climate models for the mid-Pliocene warm period. Nat. Commun. 7, 10646. https://doi.org/10.1038/ncomms10646.

Haywood, A.M., Dowsett, H.J., Dolan, A.M., Chandler, M.A., Hunter, S.J., Lunt, D.J., 2016b. The Pliocene Model Intercomparison Project (PlioMIP) Phase 2: scientific objectives and experimental design. Clim. Past 12 (3), 663. https://doi.org/10.5194/cp-12-663-2016.

Head, M.J., Norris, G., Mudie, P.J., 1989. New species of dinocysts and a new species of acritarch from the upper Miocene and lowermost Pliocene, ODP Leg 105, Site 646, Labrador Sea. Proc. Ocean Drill. Program Sci. Results 105, 453–466.

Head, M.J., 1998. Pollen and dinoflagellates from the Red Crag at Walton-on-the-Naze, Essex: evidence for a mild climatic phase during the early Late Pliocene of eastern England. Geol. Mag. 135 (6), 803–817.

Hennissen, J.A., Head, M.J., De Schepper, S., Groeneveld, J., 2017. Dinoflagellate cyst paleoecology during the Pliocene–Pleistocene climatic transition in the North Atlantic. Palaeogeogr. Palaeoclimatol. Palaeoecol. 470, 81–108. https://doi.org/10.1016/j.palaeo.2016.12.023.

Herbert, T.D., Peterson, L.C., Lawrence, K.T., Liu, Z., 2010. Tropical ocean temperatures over the past 3.5 million years. Science 328 (5985), 1530–1534. https://doi.org/10.1126/science.1185435.

Herfort, L., Schouten, S., Boon, J.P., Woltering, M., Baas, M., Weijers, J., Sinninghe Damsté, J.S., 2006. Characterization of transport and deposition of terrestrial organic matter in the southern North Sea using the BIT index. Limnol. Oceanogr. 51, 2196–2205. https://doi.org/10.4319/lo.2006.51.5.2196.

Hodgson, G.E., Funnell, B.M., 1987. Foraminiferal biofacies of the early Pliocene Coralline Crag. In: Hart, M.B. (Ed.), Micropalaeontology of Carbonate Environments, British Micropalaeontological Society Special Publication. Ellis Harwood, Chichester, UK, pp. 44–73.

Hopmans, E.C., Weijers, J.W., Schefuß, E., Herfort, L., Sinninghe Damsté, J.S., Schouten, S., 2004. A novel proxy for terrestrial organic matter in sediments based on branched and isoprenoid tetraether lipids. Earth Planet. Sci. Lett. 224, 107–116. https://doi.org/10.1016/j.epsl.2004.05.012.

Hopmans, E.C., Schouten, S., Sinninghe Damsté, J.S., 2016. The effect of improved chromatography on GDGT-based palaeoproxies. Org. Geochem. https://doi.org/10.1016/j.orggeochem.2015.12.006.

Huguet, C., Hopmans, E.C., Febo-Ayala, W., Thompson, D.H., Sinninghe Damsté, J.S., Schouten, S., 2006. An improved method to determine the absolute abundance of glycerol dibiphytanyl glycerol tetraether lipids. Org. Geochem. 37, 1036–1041. https://doi.org/10.1016/j.orggeochem.2006.05.008.

Janssen, N., Dammers, G., 2008. Sample Processing for Pre-Quaternary Palynology. Internal TNO Report.

Johnson, A.L., Hickson, J.A., Bird, A., Schöne, B.R., Balson, P.S., Heaton, T.H., Williams, M., 2009. Comparative sclerochronology of modern and mid-Pliocene (c. 3.5 Ma) Aequipecten opercularis (Mollusca, Bivalvia): an insight into past and future climate change in the north-east Atlantic region. Palaeogeogr. Palaeoclimatol. Palaeoecol. 284 (3), 164–179. https://doi.org/10.1016/j.palaeo.2009.09.022.

Jimenez-Moreno, G., Head, M.J., Harzhauser, M., 2006. Early and Middle Miocene dinoflagellate cyst stratigraphy of the central Paratethys, central Europe. J. Micropaleontol. 25 (2), 113–139. https://doi.org/10.1144/jm.25.2.113.

Knox, R.W.O'B., Bosch, J.H.A., Rasmussen, E.S., Heilmann-Clausen, C., Hiss, M., De Lugt, I.R., Kasiński, J., King, C., Köthe, A., Słodkowska, B., Standke, G., Vandenberghe, N., 2010. Cenozoic. In: Doornenbal, J.C., Stevenson, A.G. (Eds.), Petroleum Geological Atlas of the Southern Permian Basin Area. EAGE Publications b.v., Houten, pp. 211–223.

Kuhlmann, G., Langereis, C., Munsterman, D., van Leeuwen, R.J., Verreussel, R., Meulenkamp, J., Wong, T., 2006. Chronostratigraphy of Late Neogene sediments in the southern North Sea Basin and paleoenvironmental interpretations. Palaeogeogr. Palaeoclimatol. Palaeoecol. 239, 426–455. https://doi.org/10.1016/j.palaeo.2006.02.004.

Lisiecki, L.E., Raymo, M.E., 2005. A Pliocene–Pleistocene stack of 57 globally distributed benthic $\delta^{18}O$ records. Paleoceanography 20 (1). https://doi.org/10.1029/2004PA001071.

Louwye, S., Head, M.J., De Schepper, S., 2004. Dinoflagellate cyst stratigraphy and palaeoecology of the Pliocene in northern Belgium, southern North Sea Basin. Geol. Mag. 141, 353–378. https://doi.org/10.1017/S0016756804009136.

Louwye, S., De Schepper, S., 2010. The Miocene–Pliocene hiatus in the southern North Sea Basin (northern Belgium) revealed by dinoflagellate cysts. Geol. Mag. 147 (5), 760–776. https://doi.org/10.1017/S0016756810000191.

Masson-Delmotte, V., Schulz, M., Abe-Ouchi, A., Beer, J., Ganopolski, A., González Rouco, J.F., Jansen, E., Lambeck, K., Luterbacher, J., Naish, T., Osborn, T., Otto-Bliesner, B., Quinn, T., Ramesh, R., Rojas, M., Shao, X., Timmermann, A., 2013. Information from Paleoclimate Archives. In: Stocker, T.F., Qin, D., Plattner, G.-K., Tignor, M., Allen, S.K., Boschung, J., Nauels, A., Xia, Y., Bex, V., Midgley, P.M. (Eds.), Climate Change 2013: The Physical Science Basis. Contribution of Working Group I to the Fifth Assessment Report of the Intergovernmental Panel on Climate Change. Cambridge University Press, Cambridge, United Kingdom and New York, NY, USA.

Meijer, T., Cleveringa, P., Munsterman, D.K., Verreussel, R.M.C.H., 2006. The Early Pleistocene Praetiglian and Ludhamian pollen stages in the North Sea Basin and their relationship to the marine isotope record. J. Quat. Sci. 21, 307–310. https://doi.org/10.1002/jqs.956.

Ménot, G., Bard, E., Rostek, F., Weijers, J.W., Hopmans, E.C., Schouten, S., Sinninghe Damsté, J.S., 2006. Early reactivation of European rivers during the last deglaciation. Science 313, 1623–1625. https://doi.org/10.1126/science.1130511.

Mosbrugger, V., Utescher, T., Dilcher, D.L., 2005. Cenozoic continental climatic evolution of Central Europe. Proc. Natl. Acad. Sci. USA 42, 14964–14969. https://doi.org/10.1073/pnas.0505267102.

Mudelsee, M., Raymo, M.E., 2005. Slow dynamics of the Northern Hemisphere glaciation. Paleoceanography 20 (4). https://doi.org/10.1029/2005PA001153.

Mudie, P.J., 1987. Palynology and dinoflagellate biostratigraphy of Deep-Sea Drilling ProjecT LEG-94, SITE-607 and SITE-611, North-Atlantic Ocean. Init. Rep. Deep Sea Drill. Project 94, 785.

Naish, T.R., Wilson, G.S., 2009. Constraints on the amplitude of Mid-Pliocene (3.6–2.4 Ma) eustatic sea-level fluctuations from the New Zealand shallow-marine sediment record. Philos. Trans. R. Soc., Math. Phys. Eng. Sci. 367 (1886), 169–187. https://doi.org/10.1098/rsta.2008.0223.

Noorbergen, L.J., Lourens, L.J., Munsterman, D.K., Verreussel, R.M.C.H., 2015. Stable isotope stratigraphy of the early Quaternary of borehole Noordwijk, southern North Sea. Quat. Int. 386, 148–157. https://doi.org/10.1016/j.quaint.2015.02.045.

Peterse, F., Kim, J.H., Schouten, S., Kristensen, D.K., Koç, N., Sinninghe Damsté, J.S., 2009. Constraints on the application of the MBT/CBT palaeothermometer at high latitude environments (Svalbard, Norway). Org. Geochem. 40, 692–699. https://doi.org/10.1016/j.orggeochem.2009.03.004.

Peterse, F., van der Meer, J., Schouten, S., Weijers, J.W., Fierer, N., Jackson, R.B., Kim, J.H., Sinninghe Damsté, J.S., 2012. Revised calibration of the MBT–CBT paleotemperature proxy based on branched tetraether membrane lipids in surface soils. Geochim. Cosmochim. Acta 96, 215–229.

Pope, V.D., Gallani, M.L., Rowntree, P.R., Stratton, R.A., 2000. The impact of new physical parametrizations in the Hadley Centre climate model: HadAM3. Clim. Dyn. 16 (2), 123–146. https://doi.org/10.1007/s003820050009.

Pross, J., Klotz, S., 2002. Palaeotemperature calculations from the Praetiglian/Tiglian (Plio–Pleistocene) pollen record of Lieth, northern Germany: implications for the climatic evolution of NW Europe. Glob. Planet. Change 34 (3), 253–267. https://doi.org/10.1016/S0921-8181(02)00119-4.

Raymo, M.E., Lisiecki, L.E., Nisancioglu, K.H., 2006. Plio–Pleistocene ice volume, Antarctic climate, and the global δ^{18}O record. Science 313, 492–495. https://doi.org/10.1126/science.1123296.

Reuter, H.I., Lado, L.R., Hengl, T., Montanarella, L., 2008. Continental-scale digital soil mapping using European soil profile data: soil pH. Hambg. Beitr. Phys. Geogr. Landschaftsökol. 19, 91–102.

Salzmann, U., Haywood, A.M., Lunt, D.J., Valdes, P.J., Hill, D.J., 2008. A new global biome reconstruction and data-model comparison for the middle Pliocene. Glob. Ecol. Biogeogr. 17 (3), 432–447. https://doi.org/10.1111/j.1466-8238.2008.00381.x.

Salzmann, U., Dolan, A.M., Haywood, A.M., Chan, W.L., Voss, J., Hill, D.J., Contoux, C., 2013. Challenges in quantifying Pliocene terrestrial warming revealed by data-model discord. Nat. Clim. Change 3 (11), 969–974. https://doi.org/10.1038/nclimate2008.

Schreck, M., Matthiessen, J., Head, M.J., 2012. A magnetostratigraphic calibration of Middle Miocene through Pliocene dinoflagellate cyst and acritarch events in the Iceland Sea (Ocean Drilling Program Hole 907A). Rev. Palaeobot. Palynol. 187, 66–94. https://doi.org/10.1016/j.revpalbo.2012.08.006.

Sinninghe Damsté, J.S., Schouten, S., Hopmans, E.C., van Duin, A.C., Geenevasen, J.A., 2002. Crenarchaeol the characteristic core glycerol dibiphytanyl glycerol tetraether membrane lipid of cosmopolitan pelagic crenarchaeota. J. Lipid Res. 43, 1641–1651. https://doi.org/10.1194/jlr.M200148-JLR200. doi.

Sinninghe Damsté, J.S., 2016. Spatial heterogeneity of sources of branched tetraethers in shelf systems: the geochemistry of tetraethers in the Berau River delta (Kalimantan, Indonesia). Geochim. Cosmochim. Acta. https://doi.org/10.1016/j.gca.2016.04.033.

St John, K.E., Krissek, L.A., 2002. The late Miocene to Pleistocene ice-rafting history of southeast Greenland. Boreas 31 (1), 28–35. https://doi.org/10.1111/j.1502-3885.2002.tb01053.x.

Tyson, R.V., 1995. Sedimentary Organic Matter. Organic Facies and Palynofacies, first ed. Chapman & Hall, London.

Uhl, D., Klotz, S., Traiser, C., Thiel, C., Utescher, T., Kowalski, E., Dilcher, D.L., 2007. Cenozoic paleotemperatures and leaf physiognomy—a European perspective. Palaeogeogr. Palaeoclimatol. Palaeoecol. 248 (1), 24–31. https://doi.org/10.1016/j.palaeo.2006.11.005.

Utescher, T., Mosbrugger, V., Ashraf, A.R., 2000. Terrestrial climate evolution in northwest Germany over the last 25 million years. Palaios 15 (5), 430–449. https://doi.org/10.1669/0883-1351(2000)015<0430:TCEING>2.0.CO;2.

Van Adrichem Boogaert, H.A., Kouwe, W.F.P., 1993–1997. Stratigraphic nomenclature of the Netherlands; revision and update by RGD and NOGEPA.

van Engelen, A.F., Buisman, J., Ijnsen, F., 2001. A millennium of weather, winds and water in the low countries. In: Jones, P.D., Ogilvie, A.E.J., Davies, T.D., Briffa, K.R. (Eds.), History and Climate. Springer, US, pp. 101–124.

Verschuren, D., Sinninghe Damste, J.S., Moernaut, J., Kristen, I., Blaauw, M., Fagot, M., Haug, G.H., CHALLACEA project members, 2009. Half-precessional dynamics of monsoon rainfall near the East African Equator. Nature 462, 637–641. https://doi.org/10.1038/nature08520.

Warden, L., Jung-Hyun, K., Zell, C., Vis, G.J., de Stigter, H., Bonnin, J., Sinninghe Damsté, J.S., 2016. Examining the provenance of branched GDGTs in the Tagus River drainage basin and its outflow into the Atlantic Ocean over the Holocene to determine their usefulness for paleoclimate applications. Biogeosciences 13 (20), 5719. https://doi.org/10.5194/bg-13-5719-2016.

Weijers, J.W., Schouten, S., van den Donker, J.C., Hopmans, E.C., Sinninghe Damsté, J.S., 2007a. Environmental controls on bacterial tetraether membrane lipid distribution in soils. Geochim. Cosmochim. Acta 71, 703–713. https://doi.org/10.1016/j.gca.2006.10.003.

Weijers, J.W., Schefuß, E., Schouten, S., Sinninghe Damsté, J.S., 2007b. Coupled thermal and hydrological evolution of tropical Africa over the last deglaciation. Science 315 (5819), 1701–1704. https://doi.org/10.1126/science.1138131.

Williams, G.L., Fensome, R.A., MacRae, R.A., 2017. The Lentin and Williams index of fossil dinoflagellates 2004 edition. Contrib. Ser., Am. Assoc. Stratigr. Palynol. 42, 909.

Wong, T.E., Batjes, D.A., de Jager, J. (Eds.), 2007. Geology of the Netherlands. Royal Netherlands Academy of Arts and Sciences, Amsterdam.

Zagwijn, W.H., 1963. Pollen-analytic investigations in the Tiglian of the Netherlands. Geol. Stichting Meded. 16, 49–69.

Zell, C., Kim, J.H., Abril, G., Sobrinho, R.L., Dorhout, D., Moreira-Turcq, P., Sinninghe Damsté, J.S., 2013a. Impact of seasonal hydrological variation on the distributions of tetraether lipids along the Amazon River in the central Amazon basin: implications for the MBT/CBT paleothermometer and the BIT index. Front. Microbiol. 4. https://doi.org/10.3389/fmicb.2013.00228.

Zell, C., Kim, J.H., Moreira-Turcq, P., Abril, G., Hopmans, E.C., Bonnet, M.P., Sobrinho, R.L., Sinninghe Damsté, J.S., 2013b. Disentangling the origins of branched tetraether lipids and crenarchaeol in the lower Amazon River: implications for GDGT-based proxies. Limnol. Oceanogr. 58, 343–353. https://doi.org/10.4319/lo.2013.58.1.0343.

Zell, C., Kim, J.H., Dorhout, D., Baas, M., Sinninghe Damsté, J.S., 2015. Sources and distributions of branched tetraether lipids and crenarchaeol along the Portuguese continental margin: implications for the BIT index. Cont. Shelf Res. 96, 34–44. https://doi.org/10.1016/j.csr.2015.01.006.